

Polyoxometalate complexes for oxidative kinetic resolution of secondary alcohols: unique effects of chiral environment, immobilization and aggregation†

Cite this: *Dalton Trans.*, 2014, **43**, 9177

Lei Shi, Yizhan Wang, Bao Li* and Lixin Wu*

In this paper, the chiral surfactants bearing two long alkyl chains with hydroxyl groups at their terminals were synthesized and employed to encapsulate a catalytically efficient polyoxometalate through electrostatic interaction. The obtained chiral surfactant-encapsulated polyoxometalate complexes, in which a defined chiral microenvironment surrounds the inorganic cluster, were covalently immobilized into the silica matrix *via* a sol–gel process. Kinetic resolution of racemic aromatic alcohols was selected as the model reaction to evaluate the chiral supramolecular hybrid catalysts. Up to 89% enantiomeric excess was obtained by varying the reaction conditions. Importantly, the change of loading values of the chiral surfactant-encapsulated polyoxometalates leads to mutative inner microstructures ranging from uniform dispersion to subsequent formation of nanocrystalline domains in the silica matrix. Such a structural evolution differentiates the density and stability of the chiral microenvironment, resulting in a regular change of enantioselectivity of the prepared asymmetric catalysts. Moreover, the fixation of the chiral microenvironment surrounding the polyoxometalates by covalent immobilization was proved to have a promoting effect on enantioselectivity. The present research uncovers the unique effect of immobilization on the kinetic resolution. The strategy helps to understand the influencing factors of enantioselectivity, and provides a convenient and efficient approach for the construction of supramolecular asymmetric catalysts based on chiral surfactant-encapsulated polyoxometalate complexes.

Received 12th March 2014,
Accepted 11th April 2014

DOI: 10.1039/c4dt00742e

www.rsc.org/dalton

Introduction

Polyoxometalates (POMs) are a class of nano-sized inorganic clusters presenting abundant potential in the fields of chemistry, nanotechnology, and materials science.¹ Owing to their intrinsic redox and acidic properties, POMs have also been used in catalysis, especially in organic synthesis and molecular transformation.² On the other hand, chiral compounds are becoming more important in fundamental research and industrial preparation such as drug production.³ Therefore, it is of practical significance to combine the high catalytic efficiency of POMs with asymmetric catalysis.⁴ Much effort has been made to prepare chiral POMs and their derivatives in targeting the purpose,⁵ though it is less successful in making stable chiral POMs in solutions because of the rapid racemization of chiral architectures.⁶ To obtain stable chiral POM structures

under catalytic conditions, two valuable methods are adopted. One is to directly graft a chiral organic unit into POMs chemically. But in most cases, the POMs possessing highly efficient catalytic properties are hard to graft a chiral group covalently due to the structural limit, so that most of them are not suitable for this strategy. Even so, the known compounds could still not provide a high enantioselectivity in asymmetric catalysis.⁷ The other method is the encapsulation of chiral cations to achiral POM clusters. For example, chiral dendritic surfactants were used to replace the counterions of $\{\text{PO}_4[\text{WO}(\text{O}_2)_2]_4\}^{3-}$ clusters for asymmetric oxidation of sulfides and epoxidation of olefins though the enantiomeric excess (ee) was not high.⁸ A subsequent improvement largely increased the ee value of oxidized thioethers by using chiral amphiphilic cations bearing two stereocenters to enwrap a POM cluster.⁹ However, some new challenges are still inevitable: (1) the kinetic resolution in the catalytic process of chiral POM complexes has not yet been dealt with; (2) the key factors influencing the enantioselectivity are not studied in detail; and (3) the efficient separation of chiral POM catalysts is not involved in the reactions.

Because the encapsulation of organic cations to POMs is derived from the electrostatic interaction, all polyanion

State Key Laboratory of Supramolecular Structure and Materials, College of Chemistry, Jilin University, Changchun 130012, China. E-mail: wulx@jlu.edu.cn; Fax: +86-431-8519-3421; Tel: +86-431-8516-8481

†Electronic supplementary information (ESI) available. See DOI: 10.1039/c4dt00742e

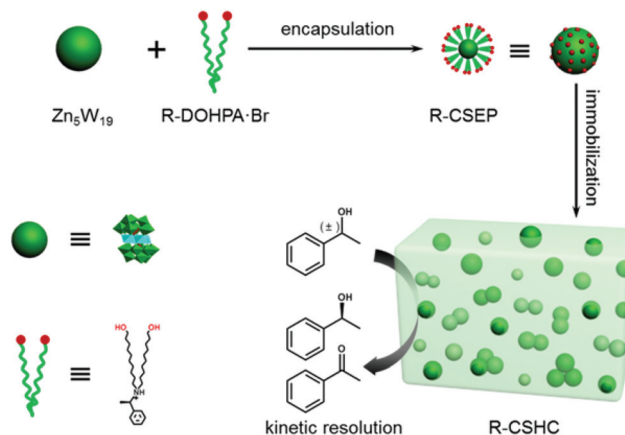
clusters are propitious to this route in principle. The formed surfactant-encapsulated POM (SEP) complexes exhibit core-shell structure similar to reverse micelles, endowing them with a good solubility in weakly polar organic solvents.¹⁰ Organic substrates can go through the hydrophobic layer to POMs, conducting the catalytic reaction. The diverse self-assembling morphologies of SEP complexes such as lamellar, nanotube, nanocone and so on are obtained under controllable conditions,¹¹ which could proceed or block the catalytic process. Through covalent immobilization into the silica, the assemblies could be disassembled and discrete SEPs disperse in the solid matrix due to the stronger chemical binding force in comparison to weak intermolecular interaction, leading to more efficient oxidation of alkenes, alcohols, and sulfides.¹² Besides, these immobilized catalysts, in which the POMs are fixed in a hydrophobic microenvironment, still have effective capability as occurred in a homogeneous system while they can be separated conveniently. Significantly, the microenvironment around achiral POMs has been applied for the improvement of asymmetric catalysis. Due to multiple catalytic sites of the POMs, the coverage density of chiral surfactants was proved to be an important factor for increasing the enantioselectivity.⁹ Notably, the chiral surfactant cations that surround the surface of POM clusters could make the chiral sites separate from the catalytic center, which largely decreases the efficiency of the chiral microenvironment.¹³ To identify this speculation, it is necessary to develop a new approach that can stabilize a chiral microenvironment. We envision that the flowing nature of chiral surfactants could be greatly suppressed by covalent immobilization of POM complexes into silica through reaction of end-groups of surfactants, which is beneficial for stabilizing the chiral microenvironment and thus promoting enantioselectivity.

We herein designed and synthesized new cationic surfactants that bear chiral head and hydroxyl groups at hydrophobic ends to encapsulate the POM with highly efficient catalytic activity. The obtained chiral SEP (CSEP) complexes are then covalently immobilized into the silica matrix through a sol-gel process, giving a series of chiral supramolecular hybrid catalysts (CSHCs) with different loading contents. The kinetic resolution of CSHCs for aromatic secondary alcohols, which is meaningful for the preparation of chiral aromatic alcohol derivatives, especially in pharmaceutical synthesis,¹⁴ is selected as a model reaction to evaluate enantioselectivity (Scheme 1). Up to 89% ee of the remaining substrates is realized under the optimized reaction conditions. Considering the simplicity and controllability of this approach, these fixed CSHCs represent a promising type of chiral POM catalysts in asymmetric organic synthesis and biological mimic systems.

Experimental

Materials

$\text{Na}_{12}[\text{WZn}_3(\text{H}_2\text{O})_2(\text{ZnW}_9\text{O}_{34})_2]\cdot 46\text{H}_2\text{O}$ was synthesized according to the published procedure.¹⁶ 11-Bromoundecan-1-ol



Scheme 1 Schematic representation for the preparation of chiral POM complex catalysts (*R*-CSHC as an example) and the loading in silica for the kinetic resolution reaction of racemic secondary alcohols.

(98%) and *N*-ethyl-*N*-isopropylpropan-2-amine (99%) were obtained from J&K Scientific Ltd. (*R*)-1-Phenylethanamine (99%, 99% ee), (*S*)-1-phenylethanamine (98%, 98% ee), cumyl hydroperoxide (80–85 wt%), *tert*-butyl hydroperoxide (70 wt% in H_2O), 1-phenylethanol (98%), 1-phenylpropanol (97%) and benzoin (99.5%) were purchased from Aladdin. Hydrogen peroxide (30% aqueous solution) and TEOS were of analytical grade and the product of Beijing Chemical Reagents Company. TEOS was distilled before use. All the solvents used in catalytic reactions were of analytical grade. Doubly distilled water was used in the experiments.

Synthesis of *R*- and *S*-DOHPA-Br

The *R*-DOHPA-Br and *S*-DOHPA-Br were synthesized following the same procedures and confirmed by FT-IR and ^1H NMR spectra and ESI-MS. By taking *R*-DOHPA-Br as an example: *N*-ethyl-*N*-isopropylpropan-2-amine (1.84 mL, 10.5 mmol) and 11-bromoundecan-1-ol (2.65 g, 10.5 mmol) were added into the acetonitrile solution (5 mL) that dissolves (*R*)-1-phenylethanamine (0.5 mL, 3.9 mmol). After stirring for 96 h at 40 °C, the reaction mixture was cooled to room temperature and the solvent was removed under reduced pressure. The residue was extracted with diethyl ether, washed with water and then dried over anhydrous MgSO_4 . The crude *R*-DOHPA-Br was dissolved in ethanol, and protonated with hydrochloric acid. The formed light yellow oily product was then separated in a yield of 39.0%. ^1H NMR (500 MHz, CD_3CN , 25 °C, TMS, ppm): δ = 1.12–2.50 (m, 36H), 1.77 (d, 3H), 2.56 (t, 2H), 2.69 (s, 1H), 2.90 (s, 1H), 3.11 (broad, 2H), 3.50 (broad, 4H), 4.37 (t, 1H), 7.46–7.80 (m, 5H), and 11.52 (broad, 1H). ESI-MS (m/z): 462.3 [M^+]. IR (KBr pellet): ν = 3408, 2925, 2854, 2644, 1460, 1385, 1059, 765, and 704 cm^{-1} . Similarly, *S*-DOHPA-Br (0.75 g) was prepared in a yield of 41.8%. ESI-MS (m/z): 462.1 [M^+]. IR (KBr pellet): ν = 3408, 2925, 2854, 2644, 1460, 1386, 1059, 766, and 704 cm^{-1} .

Preparation of *R*- and *S*-CSEP

R-CSEP and *S*-CSEP were prepared following the same procedures and confirmed by FT-IR and ^1H NMR spectra and EA and TGA measurements. For the preparation of *R*-CSEP, to a mixed solution of water–ethanol (3 : 1 in v/v) of Zn_5W_{19} (0.12 g, 0.02 mmol) was added dropwise a mixed solution of water–ethanol (3 : 1 in v/v) of *R*-DOHPA-Br (0.1 g, 0.2 mmol), where the initial molar ratio of Zn_5W_{19} and *R*-DOHPA-Br was controlled at 1 : 10. After stirring for 2 h at 50 °C, the formed precipitate was collected by centrifugation and washed several times with deionized water. The dryness of the crude product under vacuum gives a pure yellow *R*-CSEP (0.13 g) in a yield of 74.4%. ^1H NMR (500 MHz, CD_3CN , 25 °C, TMS, ppm): δ = 1.26–1.50 (m, 39H), 2.48 (broad, 6H), 3.50 (t, 4H), 3.98 (broad, 1H), 7.27–7.42 (m, 5H). IR (KBr pellets): ν = 3408, 2926, 2854, 2661, 1630, 1460, 1385, 1312, 1211, 1057, 924, 878, 766, 704, 555, and 445 cm^{-1} . Elemental analysis (%) calcd for *R*-CSEP ($\text{C}_{360}\text{H}_{672}\text{N}_{12}\text{Zn}_5\text{W}_{19}\text{O}_{92}$, 10 461.12): C 41.33, H 6.47, N 1.61; found: C 41.69, H 6.30, N 1.65, corresponding to the chemical formula (*R*-CSEP) $_{12}\text{WZn}_3(\text{ZnW}_9\text{O}_{34})_2$. By assuming that the organic component has completely decomposed and all the inorganic residuals are WO_3 and ZnO at 800 °C, the measured residue of 44.6 wt% in total from TGA is in agreement with the calculated value of 45.6 wt% according to the *R*-CSEP formula. Similarly, *S*-CSEP (0.12 g) was obtained in a yield of 68.7%. IR (KBr pellets): ν = 3417, 2926, 2854, 2662, 1628, 1460, 1385, 1312, 1208, 1057, 924, 879, 766, 704, 557, and 459 cm^{-1} . Elemental analysis (%) calcd for *S*-CSEP ($\text{C}_{360}\text{H}_{672}\text{N}_{12}\text{Zn}_5\text{W}_{19}\text{O}_{92}$, 10 461.12): C 41.33, H 6.47, N 1.61; found: C 40.91, H 6.43, N 1.72, in good agreement with the chemical formula of (*S*-CSEP) $_{12}\text{WZn}_3(\text{ZnW}_9\text{O}_{34})_2$.

Preparation of CSHCs

By taking *R*-CSHC-30 as an example, to a mixture of ethanol (60 mL) and water (1 mL) dissolving *R*-CSEP (0.1 g) was added TEOS (0.9 g). The solution was stirred vigorously, and the resulting sol was aged for about two weeks at room temperature. After a full evaporation of solvent, a transparent solid gel was obtained. During this process, *R*-CSEPs were immobilized into the silica matrix and the product was characterized by FT-IR, EA and TGA measurements, confirming that the loading value of *R*-CSEP in the silica matrix was 30 wt%. *R*-CSHC-46, *R*-CSHC-62, and *R*-CSHC-86 were prepared and characterized according to similar procedures, except that the molar ratios of *R*-CSEP and TEOS were controlled to meet the corresponding loading values. For the *S*-CSHC-58, *S*-CSEP instead of *R*-CSEP was immobilized into the silica matrix with the loading value of 58 wt%. *R*-CSHC-0 and *R*-DOHPA/ SiO_2 were prepared by immobilizing nothing and pure *R*-DOHPA-Br into the silica matrix, respectively.

Typical catalytic procedure for kinetic resolution of 1-phenylethanol

Racemic 1-phenylethanol (0.2 mmol) and 30% H_2O_2 (2.5 equiv.) were added into CH_3CN (1 mL) in a 5 mL round

bottom flask. As an example, *R*-CSHC-62 (0.4 μmol) was added. The reaction mixture was stirred under a speed of 500 r min^{-1} at 50 °C and the reaction was monitored by TLC and HPLC. After the reaction was complete, the catalysts were recovered by filtration or centrifugation. The filtrate was evaporated under reduced pressure, and for analysis purposes, a small fraction of the products was separated by preparative silica-gel TLC. The ee value was determined by chiral HPLC on a chiralcel OD-H column, eluting with hexane–isopropanol (95 : 5) at a flow rate of 1 mL min^{-1} through a UV detector (254 nm) at 40 °C.

Typical catalytic procedure for kinetic resolution of benzoin

Racemic benzoin (0.2 mmol) and 30% H_2O_2 (2.5 equiv.) were added into CH_3CN (1 mL) in a 5 mL round bottom flask. Then *R*-CSHC-86 (0.4 μmol) was added. The reaction mixture was stirred at a speed of 500 r min^{-1} at 50 °C and the reaction was examined by TLC and HPLC. After the reaction was complete, the catalyst was recovered by filtration or centrifugation. The filtrate was evaporated under reduced pressure, and for analysis purposes, a small fraction of the products was separated by preparative silica-gel TLC. The ee value was determined by chiral HPLC on a chiralcel OD-H column, eluting with hexane–isopropanol (97.5 : 2.5) at a flow rate of 0.8 mL min^{-1} through a UV detector (254 nm) at 30 °C.

Measurements

^1H NMR spectra were recorded on a Bruker Ultra-Shield TM 500 MHz spectrometer using tetramethylsilane as an internal standard (δ = 0 ppm). FT-IR spectra were collected on a Bruker Vertex 80v spectrometer equipped with a deuterated triglycine sulfate detector (32 scans) at a resolution of 4 cm^{-1} . UV-Vis and CD spectra were recorded on a Bio-Logic MOS-450 spectropolarimeter. Organic EA was carried out on a Vario micro cube from Elementar. ESI-MS was carried out on a Thermo Fisher ITQ1100 ion trap gas chromatography-mass spectrometry. TGA was performed on a TA Instruments Q500 thermal analysis system. DLS measurements were performed using a Zetasizer NanoZS (Malvern Instruments). XPS spectra are acquired on an ESCALAB-250 spectrometer with a monochromic X-ray source (Al $\text{K}\alpha$ line, 1486.6 eV). HR-TEM, SAED, and EDX were carried out on a JEM-2100F from JEOL Ltd with an accelerating voltage of 200 kV without staining. XRD analysis was performed with a Rigaku SmartLab (3) X-ray diffractometer with $\text{Cu-K}\alpha$ radiation with a wavelength of 1.54 Å operated at 40 kV and 30 mA in Bragg–Brentano geometry. N_2 adsorption isotherms were measured with a Quantachrome Instruments Autosorb 1 analyzer. The samples were degassed at 80 °C under vacuum for more than 54 h prior to the measurements. The specific surface areas were evaluated with the BET method in the P/P_0 range 0.05–0.35. Pore size distributions were calculated from the desorption branch of the isotherms by using the BJH method. The ee values were determined by HPLC analysis using a SHIMADZU LC-20A equipped with a chiralcel OD-H column (4.6 \times 250 mm) obtained from Daicel Chemical Industries Ltd.

Results and discussion

Preparation and structural characterization of CSEPs

In order to construct an efficient asymmetric catalyst based on POMs, we select a known polyanion, $\text{Na}_{12}[\text{WZn}_3(\text{H}_2\text{O})_2(\text{ZnW}_9\text{O}_{34})_2] \cdot 46\text{H}_2\text{O}$ (Zn_5W_{19}), with high catalytic activity. *R*-Di-(11-hydroxy-undecyl)-1-phenylethyl ammonium bromide (*R*-DOHPA-Br) and *S*-di(11-hydroxyundecyl)-1-phenylethyl-ammonium bromide (*S*-DOHPA-Br) which bear a chiral head and two long alkyl chains with a hydroxyl terminal group are synthesized to serve as the chiral source. The reason why the chiral center is designed close to the ionic head is that the chiral sites could attach tightly around the POM surface in the formed complex. On the other hand, the hydroxyl groups at the hydrophobic ends can assist in the immobilization in the silica matrix by reacting with Si-OH groups hydrolyzed from tetraethyl orthosilicate (TEOS). The expected structures of *R*-DOHPA-Br and *S*-DOHPA-Br are confirmed by ^1H NMR (Fig. 1), UV-Vis (Fig. S1†), and FT-IR (Fig. S2 and Table S1†) spectra. The electrospray ionization mass spectrum (ESI-MS) (Fig. S3 and S4†) gives the weights of 462.3 and 462.1 m/z for $[\text{R-DOHPA}]^+$ and $[\text{S-DOHPA}]^+$, which are in good agreement with the calculated molecular weight, 462.7 m/z , from their formulae. The circular dichroism (CD) spectra of *R*-DOHPA-Br and *S*-DOHPA-Br (Fig. 2a) are mirror symmetric, demonstrating that they are enantiopure compounds. The CSEP electrostatic complexes are prepared by simply mixing Zn_5W_{19} polyanion with DOHPA-Brs in the mixture solvent of water and ethanol. The corresponding *R*-CSEP and *S*-CSEP are no longer soluble in water but readily dissolve in organic solvents such as ethanol, acetone and acetonitrile, implying reverse micelle-like structure of CSEPs with a hydrophilic inorganic Zn_5W_{19} core and a hydrophobic chiral organic shell.

Characteristic vibration bands attributable to Zn_5W_{19} at 924 ($\nu_{\text{as}} \text{W}=\text{O}_d$), 878 ($\nu_{\text{as}} \text{W}-\text{O}_b-\text{W}$), and 766 cm^{-1} ($\nu_{\text{as}} \text{W}-\text{O}_c-\text{W}$) are observed in the FT-IR spectrum of CSEPs (Fig. S2 and Table S1†), which ascertain the well retained framework structure of the cluster. Similar to the case of dimethyl sulfoxide

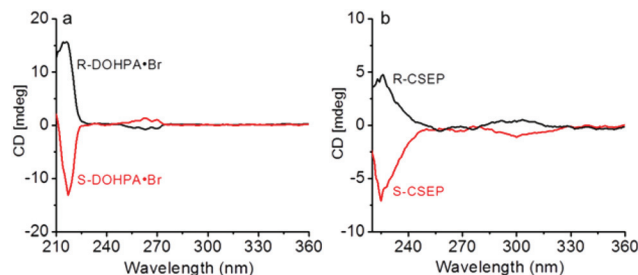


Fig. 2 CD spectra of (a) chiral organic cations, *R*-DOHPA-Br and *S*-DOHPA-Br at a concentration of 3×10^{-4} mol L^{-1} in CH_3CN , and (b) their POM complexes, *R*-CSEP and *S*-CSEP at a concentration of 2.5×10^{-5} mol L^{-1} in CH_3CN .

(DMSO) (Fig. S5†), the proton signal on chiral carbon (Hb) of $[\text{R-DOHPA}]^+$ moves from 4.37 to 3.97 ppm in CD_3CN after the encapsulation (Fig. 1 and Table S2†). Accompanied by proton signals of the $[\text{R-DOHPA}]^+$ head group shifting to higher field, the peak broadening also confirms the existence of electrostatic interaction between $[\text{R-DOHPA}]^+$ and Zn_5W_{19} polyanion. FT-IR (Fig. S6†) and UV-Vis spectra (Fig. S7†) of *R*-CSEP and *S*-CSEP are almost identical. The elemental analysis (EA) (Table S3†) and thermogravimetric analysis (TGA) (Fig. S8†) demonstrate that all counterions of the Zn_5W_{19} core are replaced by $[\text{R-DOHPA}]^+$ and $[\text{S-DOHPA}]^+$ in complexes. The estimated molecular formulae of both CSEPs are in perfect agreement with the anticipated structure: $(\text{C}_{30}\text{H}_{56}\text{NO}_2)_{12}\text{WZn}_3(\text{ZnW}_9\text{O}_{34})_2$, suggesting that one polyanion core is densely covered by twelve DOHPA surfactants on its surface due to charge neutralization.

To understand the chirality of CSEPs, the chiroptical activities of DOHPA-Brs and CSEPs are evaluated by using UV-Vis and CD spectra. The CD signals of *R*-DOHPA-Br and *S*-DOHPA-Br units are comparable to the virgin ones but shift slightly to long wavelength after their encapsulation on POMs, suggesting the influence of the electrostatic interaction on their chiroptical activities. A broad peak assigned to Zn_5W_{19} in the range between 250 and 330 nm (centered at 264 nm) appears in UV-Vis spectra of *R*- and *S*-CSEP (Fig. S7†). Correspondingly, mirror symmetric CD signals at around 300 nm are observed in CD spectra of *R*- and *S*-CSEP complexes, further confirming the influence of chirality of DOHPAs on POM clusters. The signal can be definitely assigned to the chiral induction of the organic cation to the $\text{O} \rightarrow \text{W}$ charge-transfer band of the Zn_5W_{19} cluster, according to our previous results.⁹

We also study the self-assembling behavior of *R*-CSEP both in solution and in the solid state by dynamic light scattering (DLS), X-ray diffraction (XRD) and high resolution transmission electron microscopy (HR-TEM). It is found that *R*-CSEP complexes self-aggregate in organic solvents such as ethanol, acetonitrile and acetone within variable tens of nanometers in diameter (Fig. S9–S11†). Their self-assembly in ethanol is further confirmed by HR-TEM (Fig. S12†). The spheroids in average diameter of *ca.* 110 nm, which is consist-

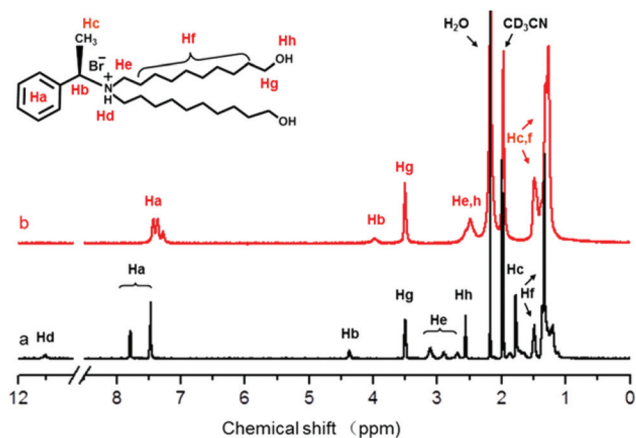


Fig. 1 ^1H NMR spectra of (a) *R*-DOHPA-Br and (b) *R*-CSEP complex in CD_3CN .

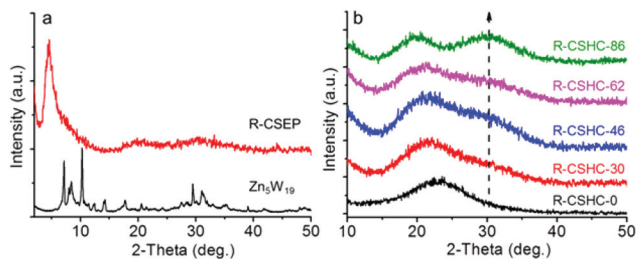


Fig. 3 (a) XRD patterns of freshly prepared solid Zn_5W_{19} and *R*-CSEP complex prepared from ethanol solution; and (b) wide angle XRD patterns of *R*-CSHC-0, *R*-CSHC-30, *R*-CSHC-46, *R*-CSHC-62 and *R*-CSHC-86.

ent with the DLS result, were found predominant. In the comparison of the rich diffraction peaks of Zn_5W_{19} in the crystalline state, the low degree of order can be observed for CSEP complexes in the solid state. As illustrated by the XRD pattern,¹⁵ only a weak peak belonging to the diffraction of CSEP complexes emerges. The calculated *d*-value is about 2.0 nm, much smaller than that of the ideal layer structure, which is rationally consistent with the disordered structure of CSEPs. The other two broad peaks at the wide angle region could be assigned to the collective reflection of Zn_5W_{19} at the corresponding region (Fig. 3a). Consistently, the detailed observation of the HR-TEM images indicates that *R*-CSEP complexes within aggregates are in a considerably disorganized state. Considering the competitive factors existing in DOHPAs, it is not surprising to get the disordered aggregation structure. Following the previous understanding, the alkyl chains in organic units should assist ordered assembly of SEPs due to the hydrophobic interaction. However, the terminal hydroxyl groups used for connecting to the silica matrix in the following sol-gel process play a destructive role in the assembly of complexes, as reported in other similar systems.¹² It is noteworthy that the single POM cluster is detectable in the HR-TEM image where the lattice fringe becomes distinguishable, which helps us to further discern the detailed aggregation morphology. The size of the single Zn_5W_{19} cluster domain is found to be in good agreement with reported data,¹⁶ and moreover, the observed lattice distances in single Zn_5W_{19} and CSEPs are calculated to be identical in 0.29 nm (Fig. 4a and 4b).

Composition and structure of CSHCs

To conduct the enantioselectivity of the designed approach for kinetic resolution, a series of CSEP-carried silica are prepared in different doping contents. By taking *R*-CSHC-30 as an example, it means that the loading of the *R*-CSEP complex in the silica matrix is 30 wt%. During the preparation of the CSHC, the calculated amount of complexes was added to the TEOS solution in proportion. The actual loading value is determined by the elemental analysis. Considering that the nitrogen element is only derived from CSEP, we calculate the loading value of the complex, which is then confirmed by the thermogravimetric analysis independently (Table S4 and Fig. S14–S18†). *R*-CSHC-46, *R*-CSHC-62, and *R*-CSHC-86 are

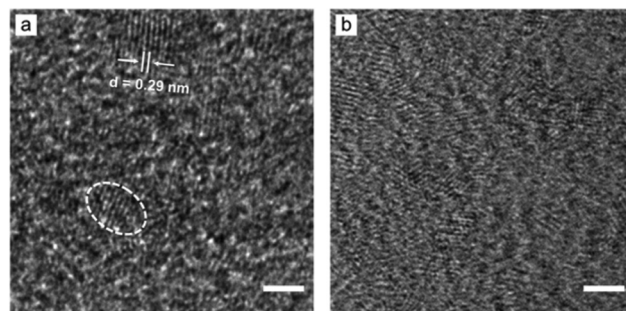


Fig. 4 HR-TEM images of (a) Zn_5W_{19} prepared from acetonitrile solution, and (b) *R*-CSEP complex prepared from ethanol solution. The circle area in (a) marks a single Zn_5W_{19} cluster domain with distinguishable lattice fringes. The scale bar is 2 nm.

prepared similarly except that the molar ratios of *R*-CSEP and TEOS are controlled to meet the expected loading content. For *S*-CSHC-58, *S*-CSEP is immobilized with the loading value of 58 wt%. As the contrast catalysts, silica *R*-CSHC-0 and *R*-DOHPA-Br-doped silica *R*-DOHPA/SiO₂ are prepared. The corresponding FT-IR and X-ray photoelectron spectroscopic (XPS) measurements further confirm the compositions and structures of the prepared CSHCs.

Besides the characteristic vibrations at 2926 and 2854 cm⁻¹ attributable to antisymmetric and symmetric CH₂ stretching of the organic component, the bands at 925 ($\nu_{as} W=O_d$), 872 ($\nu_{as} W-O_b-W$) and 775 cm⁻¹ ($\nu_{as} W-O_c-W$) can be well assigned to the vibrations of inorganic clusters. In addition to the above vibration absorptions attributed to CSEP, two additional bands emerge in IR spectra of all CSHCs (Fig. S13†). A band centered at 1080 cm⁻¹ (ν Si-O-Si) suggests the formation of a silica network, while as expected, the other band at 1163 cm⁻¹ (ν Si-O-C) confirms the covalent linkage of hydroxyl groups at the periphery of CSEPs and the silica network. The regular change in relative intensity of the characteristic vibration bands belonging to POMs and the silica network suggests the increased loadings of CSEPs. The actual loading values of CSEPs in all CSHCs are also examined by EA and TGA measurements (Table S4 and Fig. S14–S18†). For the representative *R*-CSHC-62 catalyst, the existence of elements C (1s: 284.65, 286.10, 287.83, and 288.86 eV), N (1s: 401.98 eV), and W (5p_{3/2}: 37.01 eV and 4p_{3/2}: 427.00 eV) in the X-ray photoelectron spectroscopic (XPS) measurement further confirms the incorporation of CSEP complexes into the silica matrix (Fig. S19†). The simulation for binding energy peaks belonging to the C element can be divided into four types according to their chemical environment (C-C, C-N, C-O-H and C-O-Si). The peak of the C-O-Si bond demonstrates successful condensation of the Si-OH group hydrolyzed from TEOS and terminal hydroxyl groups from the *R*-CSEP complex. Through the comparison of relative peak areas, we found that *ca.* 36.4% of OH groups on CSEP are covalently linked to the silica (Fig. S20†). That means more than four -OH groups of one CSEP are covalently linked to silica backbones on average. The incomplete immobilization of CSEP complexes could facilitate the mass

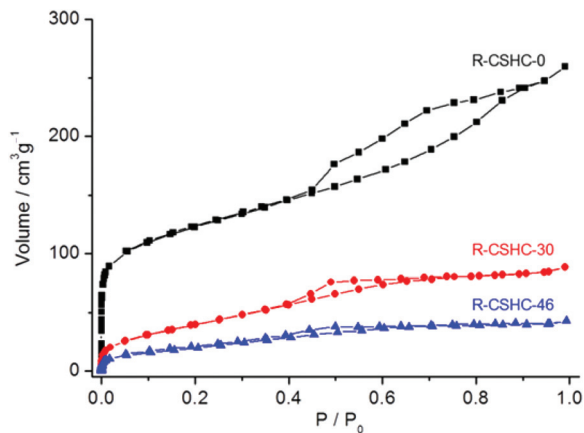


Fig. 5 Nitrogen-sorption isotherms of *R*-CSHC-0, *R*-CSHC-30 and *R*-CSHC-46.

transfer as occurred in the homogeneous catalytic process. In addition, the surface element contents of *R*-CSHC-62 and *R*-CSHC-86 are detected, and the molar ratios of Si/W, Si/C and Si/N in the latter case are all lower than those of the former (Table S5†), suggesting that a reduced amount of Si element but an increased content of W, C and N elements occurs. This implies that more CSEP complexes start to locate at the surface area of silica as their loading content increases.

Fig. 5 displays the nitrogen-sorption isotherms of CSEP-loaded silica. The corresponding pore size distribution plots of CSHCs are listed in the ESI (Fig. S21–S23†). The Brunauer–Emmett–Teller (BET) surface area of *R*-CSHC-0 is estimated to be 410 m² g⁻¹ with a total pore volume of 0.34 cm³ g⁻¹, which is well consistent with the reported data.¹⁷ After the CSEPs are loaded into the silica matrix, both the BET surface area and the total pore volume start to decrease (Table S6†), as commonly reported for the doping silica prepared by the sol-gel method.¹⁸ Thus for the samples of *R*-CSHC-30 and *R*-CSHC-46, the BET surface areas decrease greatly to 154 and 77 m² g⁻¹, respectively. The effort to get the nitrogen-sorption isotherms of both *R*-CSHC-62 and *R*-CSHC-86 does not succeed, suggesting even much lower surface areas, as expected.¹⁹ In order to ensure the efficiency and consistency for all sample entries during the catalytic process, the CSHCs are carefully ground and their representative size among hundreds of nanometers is maintained, as shown in the TEM image (Fig. S24†). Besides that, based on the characteristics of sol-gel materials, the wide pore size distribution ranging from 1 to 6 nm makes the CSHCs sufficiently allow mass transfer of organic substrates and hence contact with the CSEP catalytic center.^{12,17}

In order to figure out the induced chirality of the POMs after being immobilized into the silica, we examined the chiroptical activity of the *R*-CSHC-62 as an example (Fig. 6). The CD signal of *R*-DOHPA shifts to a long wavelength slightly, suggesting the influence of the covalent immobilization on its chiroptical activity. Importantly, the induced CD signal of POM clusters at around 300 nm is slightly enhanced, which

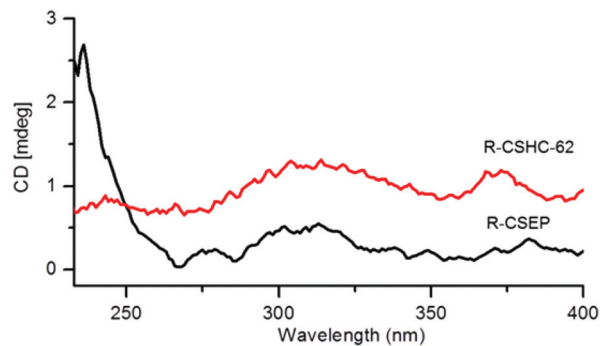


Fig. 6 CD spectrum of *R*-CSEP complexes in acetonitrile and *R*-CSHC-62 in the solid state.

could be attributed to the stabilization of the chiral micro-environment around the POM clusters. The enhancement of induced chirality of POMs by covalent immobilization should contribute to the following kinetic resolution reactions, as expected.

Kinetic resolution of racemic secondary alcohols

We select the oxidative kinetic resolution of secondary alcohols as the model reaction and some commonly used racemic secondary alcohols are used to evaluate the enantioselectivity of the CSHCs. Considering that water is the only byproduct, 30% H₂O₂ is employed as the oxidant. The reaction is performed under mild conditions (50 °C and stirring at 500 rpm) and monitored by high performance liquid chromatography (HPLC) equipped with a chiral column. The composition of products is examined by ¹H NMR and HPLC to identify the process by which the substrates are oxidized to the corresponding ketone or other possible by-products (Fig. S25–S27†).

The catalytic activity of the prepared POM complexes in silica for the oxidation of racemic 1-phenylethanol under the same reaction condition is listed in Table 1. Lower conversions and none of asymmetric oxidation are found when pure silica

Table 1 Summary of catalytic activities of different catalysts for the oxidation of racemic 1-phenylethanol^a

Entry	Sample	<i>t</i> [h]	Conv. ^b [%]	ee ^c
1	<i>R</i> -CSHC-0	72	2.9	3.3 (<i>R</i>)
2	<i>R</i> -DOHPA/SiO ₂	72	6.3	1.2 (<i>R</i>)
3	Zn ₅ W ₁₉	72	39.3	0.5 (<i>R</i>)
4	<i>R</i> -CSEP	72	25.6	5.0 (<i>R</i>)
5	<i>R</i> -CSHC-30	64	80.2	15.4 (<i>R</i>)
6	<i>R</i> -CSHC-46	64	74.5	23.9 (<i>R</i>)
7	<i>R</i> -CSHC-62	64	75.1	34.1 (<i>R</i>)
8	<i>R</i> -CSHC-86	64	71.0	38.4 (<i>R</i>)

^aAll reactions are carried out in acetonitrile (1 mL) with racemic 1-phenylethanol (0.2 mmol), 30% H₂O₂ (0.3 mmol) and the above catalysts (1 μmol) at 50 °C. ^bThe conversions are determined by HPLC based on the crude reaction mixture. ^cee values are calculated from HPLC analysis on a chiralcel OD-H column, and the absolute configuration is determined by comparison of the HPLC results with the data in the literature.²⁰

R-CSHC-0 and organic cation incorporated silica *R*-DOHPA/SiO₂ are used in the oxidation reaction. A pure Zn₅W₁₉ cluster exhibits efficient catalytic activity, suggesting its intrinsic catalytic ability to the oxidation of secondary alcohols. But it does not show any obvious chiral catalytic properties though a very small ee value appears in the results.

Interestingly, the *R*-CSEP complex exhibits a lower conversion but a higher enantioselectivity in comparison to pure Zn₅W₁₉ (Table 1, entries 3 and 4). Apparently, this change comes from the existence of a chiral microenvironment of organic components surrounding the POM surface. The electrostatic encapsulation confirms the synergetic catalysis of the chiral group and the catalytic center in the *R*-CSEP complex.⁹ The main reason for the moderate conversion using Zn₅W₁₉ as a catalyst should be the limited solubility of the naked cluster. Meanwhile, the self-aggregation of the *R*-CSEP complex leads to a restricted catalytic process, which may be responsible for the even lower conversion. Upon chemical immobilization of the *R*-CSEP complex in the silica matrix, the resulting hybrids accelerate the reaction more than 3 times compared with the complex alone within a similar reaction time (Table 1, entries 4 and 5). By comparing with the first four entries, the catalytic result of the POM complex doping in silica in entry 5 implies that: (1) CSEP aggregations in solution have broken down, providing a good dispersion of CSEP in the silica matrix; (2) the mass transfer between the POM catalytic center and substrate molecules is well maintained. The POM complexes incorporated into silica matrices also suggest their advantage in improving the reaction speed besides their easy recycling nature as a heterogeneous catalyst. More importantly, the ee value is raised to 15%, demonstrating the stabilization of the chiral microenvironment and the ensuing effect on the kinetic resolution. To examine the influence of loading content on the catalytic efficiency and enantioselectivity, we prepare a series of immobilized catalysts, *R*-CSHC-30, *R*-CSHC-46, *R*-CSHC-62 and *R*-CSHC-86. The catalytic reaction conditions are kept the same and the total amount of *R*-CSEP complexes in different catalytic reactions is controlled to be identical. As a result, though the pore volume decrease of silica under high loading of POM complexes may restrain the conversion of the substrate, the increased surface density of POM complexes on silica grains can still, in large part, compensate for the decrease of conversion. Therefore, the catalytic capability of the hybrids decreases slowly with increasing the loading of POM complexes. On the other hand, one can see a quick increase of the ee value after the chemical immobilization of chiral POM complexes in silica. With increasing the loading of POM complexes, the ee value increases quickly in the kinetic resolution of secondary alcohols. The influence of loading values on the enantioselectivity will be further discussed in the part on catalytic mechanism. Considering that the blank silica matrix *R*-CSHC-0 displays non-catalytic efficiency in the reaction, when adding the same amount of CSEP complex, the catalytic POMs in the reaction are identical, although the content of the silica matrix is different. That is, when we discuss the influence of loading values on the enantio-

Table 2 Summary of catalytic activities of *R*-CSHC-62 for the oxidation of racemic 1-phenylethanol under different reaction conditions^a

Entry	Solvent	<i>T</i> [°C]	Oxidant ^b	<i>t</i> [h]	Conv. ^c [%]	ee ^d
1	DMSO	50	1.5 (A)	64	5.1	6.7 (R)
2	Ethanol	50	1.5 (A)	64	15.2	3.4 (R)
3	Acetone	50	1.5 (A)	64	31.8	3.1 (R)
4	Toluene	50	1.5 (A)	64	66.5	3.9 (R)
5	Cyclohexane	50	1.5 (A)	64	71.7	17.6 (R)
6	Acetonitrile	50	1.5 (A)	64	73.8	32.8 (R)
7	Acetonitrile	60	1.5 (A)	64	89.1	9.8 (R)
8	Acetonitrile	40	1.5 (A)	72	24.9	4.0 (R)
9	Acetonitrile	40	2.5 (A)	70	63.9	22.9 (R)
10	Acetonitrile	50	2.5 (A)	48	64.3	37.8 (R)
11	Acetonitrile	50	5.0 (A)	24	60.1	35.1 (R)
12	Acetonitrile	50	2.5 (B)	84	15.7	10.8 (R)
13	Acetonitrile	50	2.5 (C)	96	17.7	16.0 (R)

^a All reactions are carried out with racemic 1-phenylethanol (0.2 mmol) and *R*-CSHC-62 (1 μmol) in acetonitrile (1 mL). ^b A: 30% H₂O₂, B: cumyl hydroperoxide, C: *tert*-butyl hydroperoxide. ^c The conversions are determined by HPLC based on the crude reaction mixture; ^d ee values are calculated from HPLC analysis equipped with a chiralcel OD-H column and the absolute configuration is determined by comparison of the HPLC results with the data in the literature.²⁰

selectivity, it is talking about the influence of morphological evolution resulting from loading values in CSHCs.

We use *R*-CSHC-62 to study the influence of experimental conditions on kinetic resolution. The solvents used in the catalytic reactions are found to play an important role on both the conversion and enantioselectivity. The reactions in strongly polar DMSO and ethanol lead to very low conversion and ee value (Table 2, entries 1 and 2). As the polarity decreases, the conversion increases to about 32% for the reaction in acetone while the ee value is still the same (Table 2, entry 3). Further decreasing the polarity, the conversion for the reaction in toluene and cyclohexane raises up to over 66%, but only the latter shows an obvious increase of the ee value (Table 2, entries 4 and 5). When the reaction occurs in acetonitrile, both the conversion and the ee value display an abrupt increase, and up to 33% ee value is obtained. As shown in Fig. 1 and Fig. S5,[†] we use the proton chemical shifts of *R*-DOHPA-Br and *R*-CSEP to examine the effect of environmental change on the POM surface. The proton signal of chiral carbon (H_b) in *R*-CSEP shows an up-field chemical shift corresponding to the isolated *R*-DOHPA-Br component in both DMSO-*d*₆ and CD₃CN. It is known that strong electrostatic interaction leads to an up-field chemical shift while weak interaction between organic cations and inorganic anions makes the chemical shift down-field.²¹ About two-fold chemical shift for *R*-CSEP after its encapsulation in CD₃CN to that in DMSO-*d*₆ (Table S2[†]) suggests a stronger electrostatic interaction within the *R*-CSEP complex in weakly polar solvents. These closer chiral groups to the POM should be apparently of benefit to the large increase of enantioselectivity and can well explain the first five entries in Table 2. For entry 6, it is an exception and hard to explain just following the above regularity, but the present result should be quite rational when considering the incomplete

fixation of the organic component on the silica matrix as well as the solubility and existing state of the substrate.

The temperature indicates another important factor to largely influence the conversion and enantioselectivity in the catalytic reaction. By raising the temperature from 50 °C to 60 °C, the yield of the oxidized product increases quite much whereas a great decrease of the ee value occurs (Table 2, entry 7). The result indicates that the higher temperature promotes catalytic oxidation on one side, but weakens the chiral environment attaching on the POM surface on the other side due to the decreased interaction between organic and inorganic groups. When the reaction is conducted at 40 °C, the asymmetric oxidation reaction could not proceed efficiently (Table 2, entry 8). Because a prompt decrease of conversion is accompanied by the reaction, this almost non-enantioselectivity can be apparently attributed to the lower reaction speed at this temperature. For the concentration of the oxidant, under the same conditions, more hydrogen peroxide can raise both the conversion and the ee value rapidly (Table 2, entries 8 and 9). When the oxidant increases up to 5 fold of molar equivalence of the substrate, the reaction can be carried out in a much shorter time with similar chiral products (Table 2, entries 10 and 11). According to the reported mechanism in the oxidation of alcohols by POMs, the molar ratio of the substrates to H₂O₂ is 1:1.²² The excess oxidant implies that more catalytic sites on POMs are activated at the same time, which leads to a higher possibility for one substrate molecule to be efficiently influenced by the chiral environment. But when the activated POMs are saturated, further increasing the amount of oxidant becomes no longer effective. We evaluate the peroxide, under the same reaction conditions, cumyl hydroperoxide and *tert*-butyl hydroperoxide which only give very low conversions and ee values even though the reaction extends up to 96 h (Table 2, entries 12 and 13). As summarized in Table 3, the present catalytic system demonstrates a general route for selective oxidation of racemic 1-phenylethanol and can be expanded to some other secondary alcohols. By using *R*-CSHC-62 as the catalyst, we investigate optically active remaining substrates. Only 3.4% ee is obtained for racemic 1-phenylpropanol while up to 60% ee value is acquired for

benzoin within 72 h, suggesting obvious oxidation selectivity in secondary alcohols. It is reported that more favorable interaction between the substrate and the catalyst gives higher enantioselectivity.²³ Similarly, we attribute this catalytic difference to the additional interaction between benzene rings of chiral organic cations around the POM surface and the substrate molecules containing different aromatic groups. As an example, the second benzene ring of benzoin, in comparison with 1-phenylpropanol, is favorable to yield additional interaction with chiral cations that cover POM. This enhanced absorption and getting closer to the chiral environment around the catalytic surface can be the main driving force leading to a higher enantioselectivity. *R*-CSHC-62 and *S*-CSHC-58 display comparable ee values (60% and 52% ee) at the same reaction time (Table 3, entries 2 and 3), confirming that the enantioselectivity of the CSHCs definitely originate from the chiral microenvironment around POMs. For the asymmetric catalysts with different doping contents of CSEP, *R*-CSHC-86 gives up to 56% and 89% ee values for the oxidation of 1-phenylethanol and benzoin, respectively. Compared with other *R*-CSHCs employed in the kinetic resolution, the synthesized asymmetric catalyst that contains the higher content of *R*-CSEP complex shows a corresponding higher enantioselectivity.

A kinetic study is carried out to track the course of the resolution process by employing the *R*-CSHC-86 as the catalyst (Fig. 7). The kinetic profile for the oxidation of the racemic benzoin illustrates the relationship of the reaction conversion and the corresponding ee value. According to the proceeding of the reaction, plot $\ln(C_t/C_0)$ versus reaction time t is constructed, as depicted in Fig. S28,† where C_0 and C_t represent

Table 3 Summary of the catalytic activities of CSHCs with different CSEP loading contents for different aromatic alcohols under the optimized reaction conditions^a

Entry	Catalyst	Substrate	t [h]	Conv. ^b [%]	ee ^c
1	<i>R</i> -CSHC-62	1-Phenylpropanol	72	60.1	3.4 (<i>R</i>)
2	<i>R</i> -CSHC-62	Benzoin	72	85.6	60.0 (<i>R</i>)
3	<i>S</i> -CSHC-58	Benzoin	72	80.6	51.6 (<i>S</i>)
4	<i>R</i> -CSHC-86	1-Phenylethanol	48	86.4	55.6 (<i>R</i>)
5	<i>R</i> -CSHC-86	Benzoin	72	92.1	89.4 (<i>R</i>)

^a All reactions are carried out in acetonitrile (1 mL) with racemic substrate (0.2 mmol), catalyst (1 μmol), 30% H₂O₂ (0.5 mmol) at 50 °C.

^b The conversions are determined by HPLC based on the crude reaction mixture. ^c ee values are determined by HPLC analysis on a chiralcel OD-H column and the absolute configuration is determined by comparison of the HPLC results with the data in the literature.²⁴

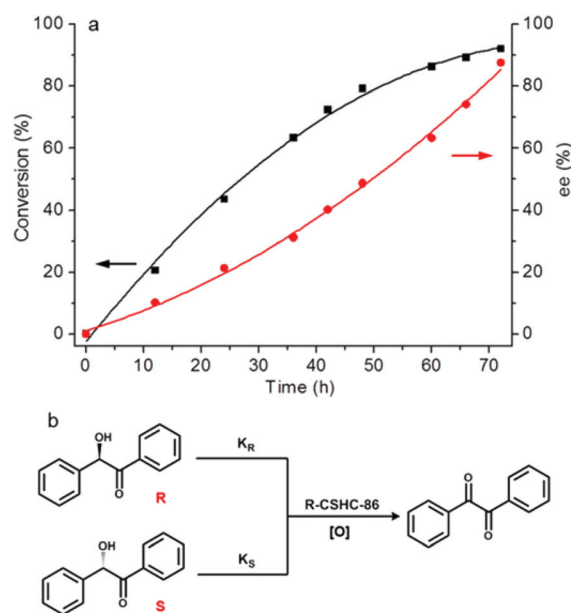


Fig. 7 (a) Time profile for the oxidation of racemic benzoin (0.2 mmol) with 30% H₂O₂ (0.5 mmol) using *R*-CSHC-86 (1 μmol) as the asymmetric catalyst in acetonitrile (1 mL) at 50 °C, and (b) the kinetic resolution process for the oxidation reaction of the racemic benzoin.

the concentrations of benzoin at the initial and intermediate states at time t , respectively. A linear relationship indicates that the reaction obeys pseudo-first-order kinetics, consistent with the result reported for a homogeneous catalytic system.²⁵ On the other hand, during the kinetic resolution process, both *R*-benzoin and *S*-benzoin transfer into the product benzil. The ee of the remaining substrates is dominated by the relative reaction rate of the enantiomers, K_R and K_S . A 10% ee value is obtained at the early stage of the reaction (10 h), but this value increases greatly to 89% after 72 h of reaction with conversion rising up to 92%. The efficient kinetic resolution suggests that K_S is faster than K_R , leading to the excess of *R*-benzoin. The rapid growth of the ee value in the catalytic process illustrates that the enantioselectivity of *R*-CSHC-86 toward benzoin is efficient.

Because of CSEP fixing in silica, the CSHC catalysts can be recovered by a simple filtration or centrifugation and the recovered CSHCs can be easily reused. FT-IR and XRD results for the catalysts after 3 cycles (Fig. S29–S30†) suggest that the structures of recovered CSHCs are well maintained though the enantioselectivity of the recovered CSHCs gradually decreases in the next catalytic process (Table S7†). TGA of the recovered CSHCs is carried out to compare its composition with that of the freshly prepared CSHCs (Fig. S31†). About 5% of outflow is estimated from the weight loss of CSEP in the recovered CSHC. Because of the much higher content of CSEP in *R*-CSHC-62, it is possible that some of POM complexes are not tightly bound to the silica matrix covalently due to only 36.4% of OH groups in the binding state. As analysed in the front part, the reduced content in the silica matrix can weaken the chiral density of the remaining complexes after the reaction, leading to the decreased ee values in the later catalysis.

Mechanism of kinetic resolution

It is obvious that the formed chiral environment of organic components attached on POMs holds the kinetic resolution process. A synergetic catalysis within the chiral POM complex has been detected, in which the POM cluster serves as the catalyst while chiral organic cations on its surface contribute to the certain enantioselectivity.⁹ Therefore, the proposed catalytic route is that the substrate molecules penetrate the organic layer and reach the POM surface, during which time they have to adopt a preferential steric conformation in the limited chiral space to accomplish the oxidation on the POM catalytic center. In other words, variable enantioselectivity is the direct result of differentiation of the chiral environment. Apparently, two main factors involving the chiral environment are the chiral density and the chiral solidity. On the one hand, due to the multiple catalytic sites on the POM cluster, relatively high chiral density of the organic layer provides more probability of substrates to be compressed in the ambience. On the other hand, the intrinsic fluid nature of the chiral cations rather than fixing at the POM surface may result in an incompletely filled chiral layer, which may decrease the opportunity of substrates to reproduce the chiral environment. Therefore, the stabilization of the chiral environment becomes crucial in pro-

moting enantioselectivity. However, the difficulty in quantitatively evaluating the density and stability of the chiral environment is still a key challenge in understanding the process. Based on the results on the kinetic resolution and characterization of *R*-CSHC, we try to provide some evidence for the abovementioned hypothesis.

HR-TEM, XRD, selected area electron diffraction (SEAD) and energy dispersive X-ray spectroscopy (EDX) are carried out to detect the inner structure of *R*-CSHCs with different *R*-CSEP loadings. The POM core in the CSEP complex has been reported to be in a dark dot like domain in TEM images and the lattice fringes could be observed in HR-TEM.²⁶ The fine structure with sizes of 1 to 2 nm (Fig. 8), as observed in *R*-CSHC-30 and *R*-CSHC-46, is consistent with that of Zn_5W_{19} clusters,¹⁶ confirming the incorporation of POMs into hybrid silica. No obvious aggregation of POMs is observed in *R*-CSHC-30 and *R*-CSHC-46, suggesting that the *R*-CSEP complexes are isolated rather than aggregated in the silica matrix. The broad reflection centered at $2\theta = 21\text{--}22^\circ$ in the XRD

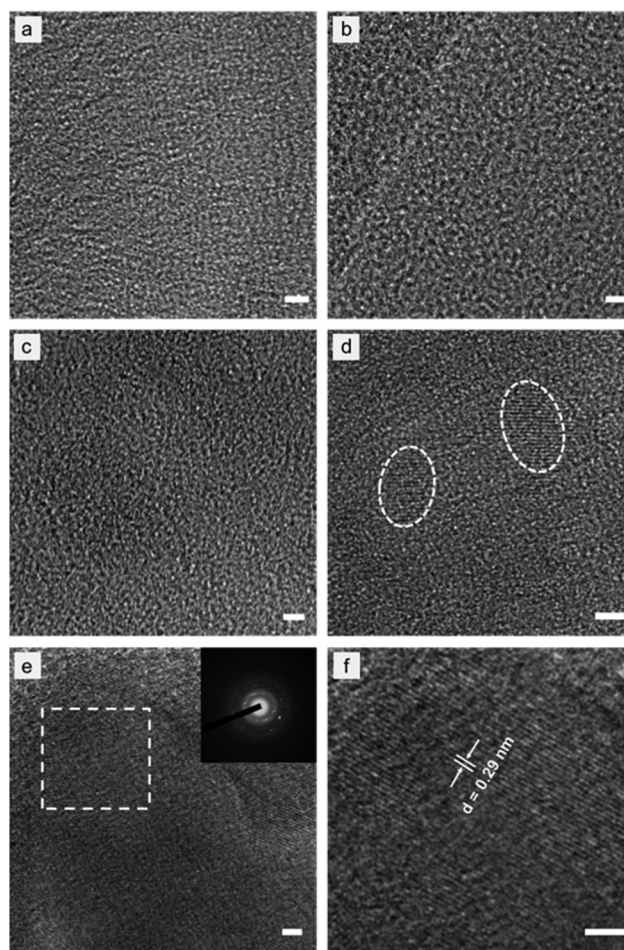
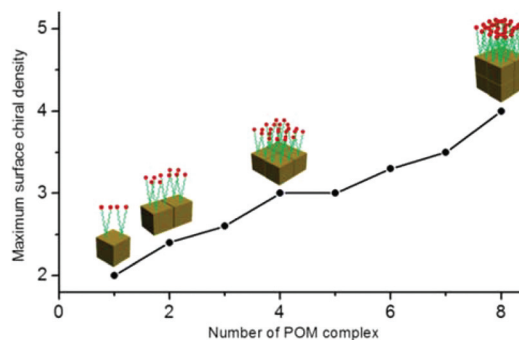


Fig. 8 HR-TEM images of (a) *R*-CSHC-0, (b) *R*-CSHC-30, (c) *R*-CSHC-46, (d) *R*-CSHC-62, (e) *R*-CSHC-86, and (f) the corresponding magnified image of the area in white box of (e). Inset in (e) is the corresponding electron diffraction pattern. The scale bars in all images are 2 nm.

patterns displays the characteristic peak of the sol-gel amorphous carrier.²⁷ The high content of the *R*-CSEP complex in silica results in the appearance of weak diffraction at small angle (Fig. S32†). Unexpectedly, small isolated nanocrystalline domains with distinguishable lattice fringes emerge in the *R*-CSHC-62 while the dark dots continue to be dominant. Moreover, the nanocrystalline domains in *R*-CSHC-86 extend into a larger area, indicative of further crystallization of the *R*-CSEP complex in the silica matrix. This could be confirmed by the EDX result (Fig. S33†). Correspondingly, a broad diffraction peak (centered at $2\theta = 30.5^\circ$) appears and becomes more and more evident as the loading value of the *R*-CSEP complex increases (Fig. 3b). This could be assigned to the peak collection of pure Zn_5W_{19} diffractions in the same region. The diffraction broadening of the corresponding peaks can be ascribed to the formation of nanocrystalline domains.²⁸ What is more, the calculated *d*-value (0.29 nm) from XRD data is in good agreement with both the lattice distance of pure Zn_5W_{19} (Fig. 4a) and that of *R*-CSHC-86 (Fig. 8f) measured in the HR-TEM image. The result further confirms the structural integrity of the Zn_5W_{19} clusters during the whole preparation process. It is noted that the size of nanocrystalline domains in the *R*-CSHC-62 and *R*-CSHC-86 remains nano-sized and the orientation of the crystalline domains is disordered, as confirmed by SAED and HR-TEM characterization (inset of Fig. 8e). The coincident evidence between the XRD pattern and the HR-TEM image points to a morphological evolution from a uniform dispersion of *R*-CSEP complexes to the formation of nanocrystalline domains in the *R*-CSHCs.

The structural characterization of the POM complex in silica provides a slot to understand the contribution of the chiral environment on the enantioselectivity and the key factors in the kinetic resolution process. As observed in the HR-TEM images, the formation of consecutive Zn_5W_{19} nanocrystalline domains in the matrix indicates the existence of POM aggregations and the tight cluster's stacking. The aggregation implies that the partial surface area of single POM cluster, at which the chiral cations locate originally, starts to become occupied by adjacent POM clusters, leading to the rearrangement of those organic components. With this understanding, we could figure out a correlation between surface chiral density around POM and the enantioselectivity (Scheme 2). To simplify the model, we assume that the POM cluster can be compressed into a cubic shape with 6 identical faces. Thus, the total chiral organic cations equally disperse on other faces when one face of a POM is covered by a face of another POM upon two clusters forming an aggregated particle. Considering the huge possibilities when different numbers of complexes aggregate together, we only analyze the surface cation density at the densest stacking state. The surface density (D_{coc}) of chiral cations (the average number of chiral organic cations on one face of a POM in an aggregated particle) for nanocrystalline particles is calculated and listed in Table S8.† The original surface density is 2 chiral organic cations on each face for the isolated CSEP complex that owns 12 organic cations. For the nanocrystalline domain containing



Scheme 2 The calculated surface density (D_{coc}) of chiral organic cations as a function of the number (N_{cc}) of *R*-CSEP chiral complexes in the formed nanocrystalline domains. The insets are the corresponding schematic evolution of the complexes in the formation of nanocrystalline domains, in which we just depict some faces of the POM cluster aggregations.

3 CSEP complexes, the surface chiral density increases to 2.6 chiral cations per POM face. In the case of a nanocrystalline domain containing 8 CSEP complexes, the surface density of the chiral cation reaches 4.0 chiral cations per POM face, twice of that in the isolated CSEP complex. From this analysis, the aggregation is obviously favourable for the increase of chiral product. Furthermore, according to total surface area based on the reported crystal data, one face area of an isolated Zn_5W_{19} is calculated to be *ca.* 2.03 nm².¹⁶ Considering the structural similarity to the present chiral cation, we use dioctadecyldimethyl ammonium with double chains and a known cross-sectional area (0.57 nm²) to evaluate the surface occupation of the chiral cations.²⁹ As a result, the surface area (S_{coc}) of chiral cations on one face is $0.57 \times D_{coc} = 1.14$ nm², much less than the maximum of a single face of Zn_5W_{19} . This lower density chiral environment well explains the lower efficiency of asymmetric catalysis under lower CSEP complex loading in silica. With increasing the aggregation number, the density of the chiral cation on Zn_5W_{19} increases, well explaining why the CSEP complex aggregation in the silica matrix can lead to an enriched chiral microenvironment and thus high enantioselectivity in the kinetic resolution. However, when the number of complexes in one nanocrystalline particle reaches 8, the chiral surface area S_{coc} will increase up to 2.28 nm², a bit larger than a single face area of an isolated Zn_5W_{19} cluster. This implies that the POM surface could not accommodate so many organic chiral cations. Because of the non-densest stacking in the practical aggregation systems, the compressibility of organic cations and the electrostatic repulsion between POMs, the number of complexes in nanocrystalline particles could be possibly more than the predicted amount. But in any case, as observed in the TEM image, the number of complexes in aggregation should be in a limited range.

Due to the steric restriction of the enriched chiral environment resulting from the decreasing surface area of the CSEP complex in aggregations, the fluidity of the rearranged chiral organic cations around the POM clusters is forced to weaken synchronously, leaving a stiffer chiral layer. Notably, the above

discussion focuses only on CSEP complex-immobilized hybrid catalysts rather than on their bulk state in the solution. Actually, a more beneficial stabilization of the chiral microenvironment in solution even provides a much higher chiral density without a stabilization strategy. But it is hard to obtain high enantioselectivity in the kinetic resolution.⁹ Though we could not quantitatively evaluate the influence of the stabilization of the chiral environment, the obvious promoting effect implies that the fixation of the chiral layer around POMs should be another critical factor for the chiral resolution of secondary alcohols.

Conclusions

In conclusion, we have systematically studied the kinetic resolution of aromatic secondary alcohols by preparing newly designed chiral POM complex-incorporated silica hybrids. This kind of CSHC hybrids that possess defined chiral microenvironment surrounding POM clusters exhibit catalytic properties like those of heterogeneous asymmetric catalysts. The kinetic resolution process is found to be closely related to the chiral density and the stabilization of the chiral layer of CSEP complexes that has covalently immobilized into the silica matrix. Besides fixation in silica, the existing state of the POM complex in CSHCs is also considered to be responsible for the corresponding promotion of the enantioselectivity in the kinetic resolution. A possible mechanism for understanding the influence of the immobilized catalysts on the enantioselectivity is proposed based on the characterization results of HR-TEM, XRD and SAED. The covalent immobilization and existing state change of the POM complex in CSHCs are proved to co-contribute to a more stable and enriched chiral microenvironment. The present research provides a convenient and effective approach to prepare asymmetric catalysts and uncovers valuable principles for developing efficient supramolecular asymmetric catalysts based on achiral POMs bearing chiral organic counterions.

Acknowledgements

This work was financially supported by the National Basic Research Program (2013CB834503), NSFC (91227110, 21221063), Ministry of Education of China (20120061110047), 111-Project (B06009) for the collaboration with WVU, and Open Project of SKL of Polymer Physics & Chemistry, CAS.

Notes and references

- M. T. Pope and A. Müller, *Angew. Chem., Int. Ed. Engl.*, 1991, **30**, 34; special issue on "polyoxometalates", *Chem. Rev.*, 1998, **98**, 1.
- K. Kamata, K. Yonehara, Y. Sumida, K. Yamaguchi, S. Hikichi and N. Mizuno, *Science*, 2003, **300**, 964; A. Haimov and R. Neumann, *J. Am. Chem. Soc.*, 2006, **128**, 15697; N. Dupré, P. Rémy, K. Micoine, C. Boglio, S. Thorimbert, E. Lacôte, B. Hasenknopf and M. Malacria, *Chem. – Eur. J.*, 2010, **16**, 7256; F. M. Toma, A. Sartorel, M. Iurlo, M. Carraro, P. Parisse, C. Maccato, S. Rapino, B. R. Gonzalez, H. Amenitsch, T. D. Ros, L. Casalis, A. Goldoni, M. Marcaccio, G. Scorrano, G. Scoles, F. Paolucci, M. Prato and M. Bonchio, *Nat. Chem.*, 2010, **2**, 826; O. A. Kholdeeva, B. G. Donoeva, T. A. Trubitsina, G. Al-Kadamany and U. Kortz, *Eur. J. Inorg. Chem.*, 2009, 5134; Y. V. Geletii, B. Botar, P. Kögerler, D. A. Hillesheim, D. G. Musaev and C. L. Hill, *Angew. Chem., Int. Ed.*, 2008, **47**, 3896.
- R. Noyori, *Angew. Chem., Int. Ed.*, 2002, **41**, 2008; Y. Huang, T. Liu, J. Lin, J. Lü, Z. Lin and R. Cao, *Inorg. Chem.*, 2011, **50**, 2191.
- B. Hasenknopf, K. Micoine, E. Lacôte, S. Thorimbert, M. Malacria and R. Thouvenot, *Eur. J. Inorg. Chem.*, 2008, 5001; D. Du, L. Yan, Z. Su, S. Li, Y. Lan and E. Wang, *Coord. Chem. Rev.*, 2013, **257**, 702.
- J. F. Garvey and M. T. Pope, *Inorg. Chem.*, 1978, **17**, 1115; H. An, E. Wang, D. Xiao, Y. Li, Z. Su and L. Xu, *Angew. Chem., Int. Ed.*, 2006, **45**, 904; H. Tan, Y. Li, Z. Zhang, C. Qin, X. Wang, E. Wang and Z. Su, *J. Am. Chem. Soc.*, 2007, **129**, 10066; Y. Hou, X. Fang and C. L. Hill, *Chem. – Eur. J.*, 2007, **13**, 9442; U. Kortz, M. G. Savelieff, F. Y. Abou Ghali, L. M. Khalil, S. A. Maalouf and D. I. Sinno, *Angew. Chem., Int. Ed.*, 2002, **41**, 4070; K. Micoine, B. Hasenknopf, S. Thorimbert, E. Lacôte and M. Malacria, *Angew. Chem., Int. Ed.*, 2009, **48**, 3466; J. Zhang, J. Hao, Y. Wei, F. Xiao, P. Yin and L. Wang, *J. Am. Chem. Soc.*, 2010, **132**, 14; F. Xiao, J. Hao, J. Zhang, C. Lv, P. Yin, L. Wang and Y. Wei, *J. Am. Chem. Soc.*, 2010, **132**, 5956.
- X. Fang, T. M. Anderson and C. L. Hill, *Angew. Chem., Int. Ed.*, 2005, **44**, 3540.
- M. Carraro, G. Modugno, A. Sartorel, G. Scorrano and M. Bonchio, *Eur. J. Inorg. Chem.*, 2009, 5164.
- C. Jahier, M. Cantuel, N. D. McClenaghan, T. Buffeteau, D. Cavagnat, F. Agbossou, M. Carraro, M. Bonchio and S. Nlate, *Chem. – Eur. J.*, 2009, **15**, 8703; C. Jahier and S. Nlate, *Eur. J. Inorg. Chem.*, 2012, 833.
- Y. Wang, H. Li, W. Qi, Y. Yang, Y. Yan, B. Li and L. Wu, *J. Mater. Chem.*, 2012, **22**, 9181.
- C. Venturello and R. D'Aloisio, *J. Org. Chem.*, 1988, **53**, 1553.
- Y. Yang, Y. Wang, H. Li, W. Li and L. Wu, *Chem. – Eur. J.*, 2010, **16**, 8062; Y. Yan, H. Wang, B. Li, G. Hou, Z. Yin, L. Wu and V. W. W. Yam, *Angew. Chem., Int. Ed.*, 2010, **49**, 9233; A. Nisar, J. Zhuang and X. Wang, *Adv. Mater.*, 2011, **23**, 1130; A. Nisar, Y. Lu, J. Zhuang and X. Wang, *Angew. Chem., Int. Ed.*, 2011, **123**, 3245.
- W. Qi, H. Li and L. Wu, *Adv. Mater.*, 2007, **19**, 1983; W. Qi, Y. Wang, W. Li and L. Wu, *Chem. – Eur. J.*, 2010, **16**, 1068.
- H. Li, H. Sun, W. Qi, M. Xu and L. Wu, *Angew. Chem., Int. Ed.*, 2007, **46**, 1300; Y. Yan and L. Wu, *Isr. J. Chem.*, 2011, **51**, 181.

- 14 S. D. Rychnovsky, T. L. McLernon and H. Rajapakse, *J. Org. Chem.*, 1996, **61**, 1194; D. C. Ebner, R. M. Trend, C. Genet, M. J. McGrath, P. O'Brien and B. M. Stoltz, *Angew. Chem., Int. Ed.*, 2008, **47**, 6367.
- 15 S. B. Yoon, J. Y. Kim and J. Yu, *Chem. Commun.*, 2001, 559.
- 16 C. M. Tourné, G. F. Tourné and F. Zonnevillje, *J. Chem. Soc., Dalton Trans.*, 1991, 143.
- 17 L. L. Hench and J. K. West, *Chem. Rev.*, 1990, **90**, 33; B. Yang, Y. Zhang, E. Drabarek, P. R. F. Barnes and V. Luca, *Chem. Mater.*, 2007, **19**, 5664.
- 18 S. Cheng, Y. Wei, Q. Feng, K. Qiu, J. Pang, S. A. Jansen, R. Yin and K. Ong, *Chem. Mater.*, 2003, **15**, 1560; F. Shi, Q. Zhang, D. Li and Y. Deng, *Chem. – Eur. J.*, 2005, **11**, 5279.
- 19 A. González-Campo, B. Boury, F. Teixidor and R. Núñez, *Chem. Mater.*, 2006, **18**, 4344; D. K. Yi, S. T. Selvan, S. S. Lee, G. C. Papaefthymiou, D. Kundaliya and J. Y. Ying, *J. Am. Chem. Soc.*, 2005, **127**, 4990.
- 20 S. Zeror, J. Collin, J.-C. Fiaud and L. Aribi-Zouiouche, *J. Mol. Catal. A: Chem.*, 2006, **256**, 85.
- 21 W. Qi, H. Li and L. Wu, *J. Phys. Chem. B*, 2008, **112**, 8257; H. Li, Y. Yang, Y. Wang, W. Li, L. Bi and L. Wu, *Chem. Commun.*, 2010, **46**, 3750; Y. Wang, H. Li, C. Wu, Y. Yang, L. Shi and L. Wu, *Angew. Chem., Int. Ed.*, 2013, **125**, 4675.
- 22 A. Haimov and R. Neumann, *J. Am. Chem. Soc.*, 2006, **128**, 15697.
- 23 F. D. Furia, G. Licini, G. Modena and R. Motterle, *J. Org. Chem.*, 1996, **61**, 5175.
- 24 C. Bolm, M. Kesselgruber, A. Grenz, N. Hermanns and J. P. Hildebrand, *New J. Chem.*, 2001, **25**, 13; M. C. Fragnelli, P. Hoyos, D. Romano, R. Gandolfi, A. R. Alcántara and F. Molinari, *Tetrahedron*, 2012, **68**, 523.
- 25 L. Ni, J. Patscheider, K. K. Baldridge and G. R. Patzke, *Chem. – Eur. J.*, 2012, **18**, 13293.
- 26 H. Nair, J. T. Miller, E. A. Stach and C. D. Baertsch, *J. Catal.*, 2010, **270**, 40.
- 27 S. C. Nunes, V. de Zea Bermudez, M. M. Silva, M. J. Smith, D. Ostrovskii, R. A. Sá Ferreira, L. D. Carlos, J. Rocha, A. Gonçalves and E. Fortunato, *J. Mater. Chem.*, 2007, **17**, 4239.
- 28 W. Ma, C. Yang, X. Gong, K. Lee and A. J. Heeger, *Adv. Funct. Mater.*, 2005, **15**, 1617.
- 29 K. Okuyama, Y. Soboi, N. Iijima, K. Hirabayashi, T. Kunitake and T. Kajiyama, *Bull. Chem. Soc. Jpn.*, 1988, **61**, 1485.